Originally Published at ISTFA 2024: Proceedings from the 50th International Symposium for Testing and Failure Analysis Conference

Consideration of a Ga-FIB in Lamella Sample Prep for EBIC/EBAC Analysis of Advanced-node SRAMs

Seeing beyond

Gregory M. Johnson, Cheryl Hartfield
ZEISS Microscopy

Andreas Rummel
Kleindiek Nanotechnik

Heiko Stegmann
Carl Zeiss Microscopy GmbH

Lorenz Lechner
Kleindiek, Inc.

Abstract

The effects of sample prep with a Ga^+-ion focused ion beam (Ga-FIB) on measurements of electron beam induced current (EBIC) were studied. Concerns have been occasionally raised about amorphization from the beam, or even Ga^+ implantation ruining the ability to make useful measurements for purposes of either failure analysis or device tailoring. To understand the magnitude of any deleterious effects, two different lamellae from a 5 nm SRAM sample were prepared with different areas of increasingly improved polish, as indicated by decreasing, cumulative, FIB beam energy, followed by EBIC measurements at 1 or 2 kV beam landing energy. A first experiment looked at the ability to generate EBIC measurements from depletion zones and found no difference across the various beam polish cells. A second experiment considered leakage and/or shorts and found little problematic currents, within standard deviations.

Introduction

Technology Challenges

As technology nodes continue to shrink, so has the need for increased resolution of failure analysis (FA) techniques to isolate failures and find defects. For the 5 nm technology node, several additional factors have been identified. There may be leakage issues associated with elongated gates and the need for taller fins also requires taller source/drain epi regions.[1] Larger effective widths may lead to fluctuations in dopant levels. Process variations, in sectors such as lithography and etch, may allow for more dopant diffusion.[2] These issues point to the possibility of increased sensitivity to implant-related leakage, and thus, the need for junction-related failure analysis techniques.

Nanoprobing is one of the highest-resolution fault isolation techniques available, as it is possible to isolate a failure to a single transistor, even in the most advanced technology nodes. For SRAM, typical FA procedures include delayering to a specific bit fail site, then performing nanoprobing operations on the six or more transistors which make up a site, and then preparing a cross section.[3-5]

Using Ga-FIB for FA of integrated circuits provides many benefits, including the ability to make cross sections at any chosen location on a die or wafer with nanoscale target accuracy. These lamellae may then be imaged with any number of analytical techniques, including transmission electron microscopy (TEM),[6] EBIC,[7] etc. Some of the concerns typically raised about the use of Ga-FIB for semiconductor FA relate to amorphization from the beam and the possibility of doping the area of interest with Ga^+ ions.[8-11] While the literature consistently reports that any amorphization layer in Si is small (only the order of one nm per kV of the applied beam), nevertheless, concerns still remain about the usage of Ga-FIB in sample prep.

EBAC and EBIC

In addition to the direct and full I-V characterization of a transistor nanoprobing provides additional opportunities for characterization of nets and *p/n* junctions. While at least nine mechanisms for generating signals in nanoprobing[12] have been identified, the methods fall into broad categories such as electron beam absorbed current (EBAC) and EBIC. A probe dropped on a sample may generate both kinds of signals, even in the same field of view.

EBAC allows the tracing of specific nets in a sample by showing the conduction paths between areas scanned by an electron beam and a probe dropped on the surface. One mode for this mechanism is shown in Figure 1. At certain beam landing energies, the surface materials may emit more secondary electrons than they received from the beam. Thus, this local charge imbalance is resupplied by the nanoprobing needle. A “negative” current is thus recorded in the system.

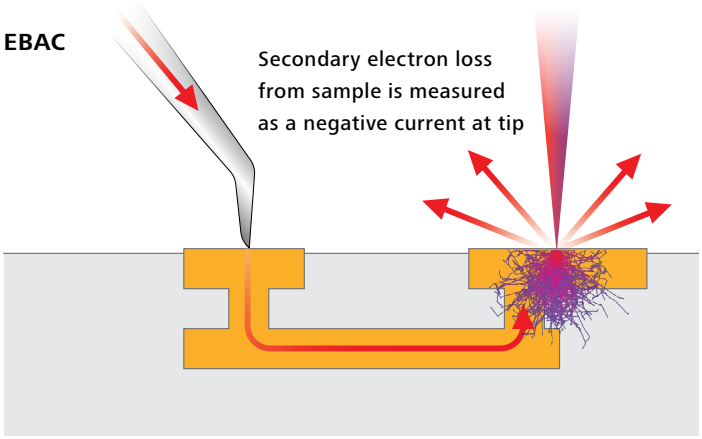

Figure 1 *Diagram of a common mechanism for the detection of EBAC currents in nanoprobing. A probe is placed on a net while the electron beam scans the sample. Loss of secondary electrons from sample is recorded as negative current by the probing system.*

EBIC, meanwhile, is a powerful technique for imaging *p/n* junctions in semiconductors.[13,14] While the probing setup is exactly the same as with EBAC, one may directly image the depletion zone of a junction. The technique is better understood by consulting the energy band diagram of a *p/n* junction, as shown in Figure 2. The depletion zone has an electric field, which intuitively may be considered as a hill along which free electrons may roll downhill, while holes are like bubbles that would float upwards. These carrier fluxes can then be measured as currents by a nanoprobing needle placed at an appropriate location in a field of view. Depending on the needle placement and the orientation of the field, the carriers may be pushed towards or away from the needle, resulting in either a positive or negative current being measured. These currents of opposite signs can easily be displayed as a color map with appropriate software.

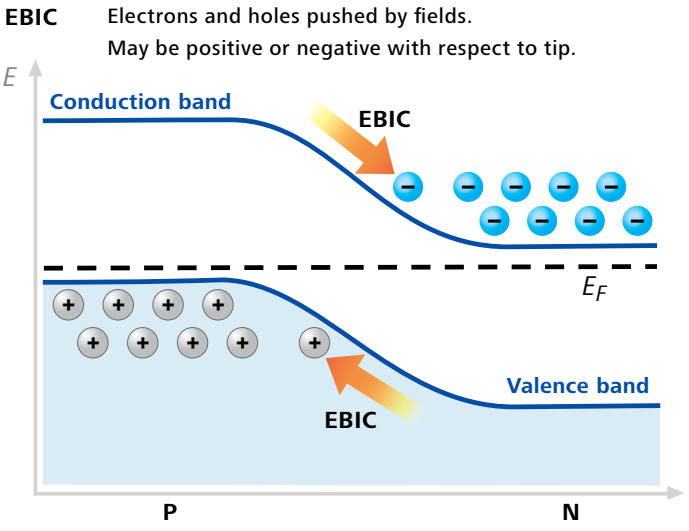

Figure 2 *Diagram explaining EBIC by means of the energy band diagram for a semiconductor. Electric fields exist at the transition between n- and p-type regions, the depletion zone. Any charge carriers introduced to or liberated in this zone are acted upon by these fields and result in currents. These currents may be recorded as positive or negative depending on their direction relative to the probe tip.*

The literature has conclusively shown that the use of Ga-FIB in sample preparation does not impact the ability to do EBIC measurements on power devices.[14,15] Additional study on silicon logic technology would be useful to those planning a FA routine due to indicators that junction profiles may become even more important to device performance in advanced nodes.[16]

Experimental

First Lamella Preparation

A commercially available 5 nm semiconductor sample containing SRAM cells was delayered to the contact level by mechanical polishing. Two different lamellae were prepared from the sample by cross-sectioning perpendicular to the fins using a ZEISS Crossbeam 550L FIB-SEM. The first lamella was approximately 15 µm long and 1 µm thick. Four different 3 µm-wide windows were created within the lamella, each using an increasing number of polishing steps with increasingly smaller FIB voltages:

- 30 kV
- 30 kV + 5 kV
- 30 kV + 5 kV + 2 kV
- 30 kV + 5 kV +2 kV + 0.5 kV

Given that the amorphization layer in a Si sample sectioned with a FIB beam is roughly equivalent in nm to the kV of the Ga^+ beam, it was expected that these four different treatments would provide regions with increasingly reduced thicknesses of amorphous beam damage. The lamella prepared by this technique is displayed in Figure 3.

The lamella was then mounted to a copper TEM sample grid by the standard *in situ* lift-out approach, using Pt precursor to perform attachment by ion beam induced deposition. The grid containing the lamella was then transferred into a ZEISS GeminiSEM 300 for SEM imaging and EBIC measurements with a Kleindiek Nanotechnik PS8e Prober Shuttle, which included an EBIC amplifier.

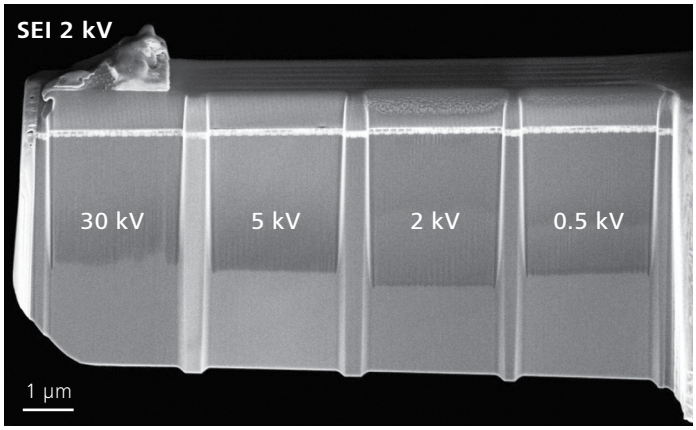

Figure 3 *SEM image of a lamella cross-section sample prepared from a 5 nm SRAM, sectioned perpendicular to the fins and wells. The label indicates the last level of Ga-FIB polish mill, in a cumulatively increasing series, that was applied to the sample.*

First Lamella Results

EBIC analysis at 2.0 kV (SEM) beam landing energy is shown in Figure 4. Across the top of the device, several black squares represent the depletion zones between the N-wells of the SRAM cells, and the surrounding P-well. While the experiment was designed to detect the degree of polish that was necessary to overcome the Ga^+ beam amorphization or implantation effects, the EBIC signals are clearly distinguishable and largely uniform across all cells — even those 13 µm away from the probe tip. There is little difference observed at this magnification between the various cells in the sample. This one image provides strong evidence that Ga-FIB milling does not prevent the collection of useful EBIC data from a lamella.

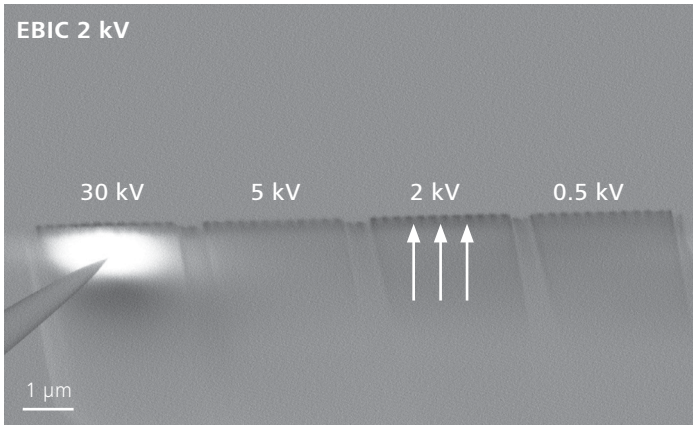

Figure 4 *EBIC analysis at 2.0 kV of the same field of view as Figure 3. A series of dark squares run across the image, indicating measurement of the N-wells (arrows). These N-well shapes are visible in every cell of the experiment. A bright plume is also seen at the location where the probe tip touches the sample. This is simply a region where there is significant path to the ground of the needle through the amplifier and does not interfere with interpretation of other features in the image.*

A large white field is also seen in the image. This is simply the region where the electrons from the incident beam find a path to ground through the tip. It does not affect the ability to image the depletion zone around the N-wells. Some regions are off scale in brightness because the amplifier settings are set to capture the range of currents which are seen in the depletion zones. These images were reported earlier,[17] but the discussion is revisited in this paper.

Figure 5 contains the results of a higher magnification scan on the sample from the cell milled only by 30 kV Ga^+ beam. The EBIC results show the N-type fins are clearly visible (red arrows), as well as the P-type (blue arrows). The diagram at the bottom of Figure 5 provides a reminder of the expected pattern. Again, to consider the purpose of this experiment, even in a cell where the surface is expected to be the most roughened, EBIC data provides direct imaging of the fins.

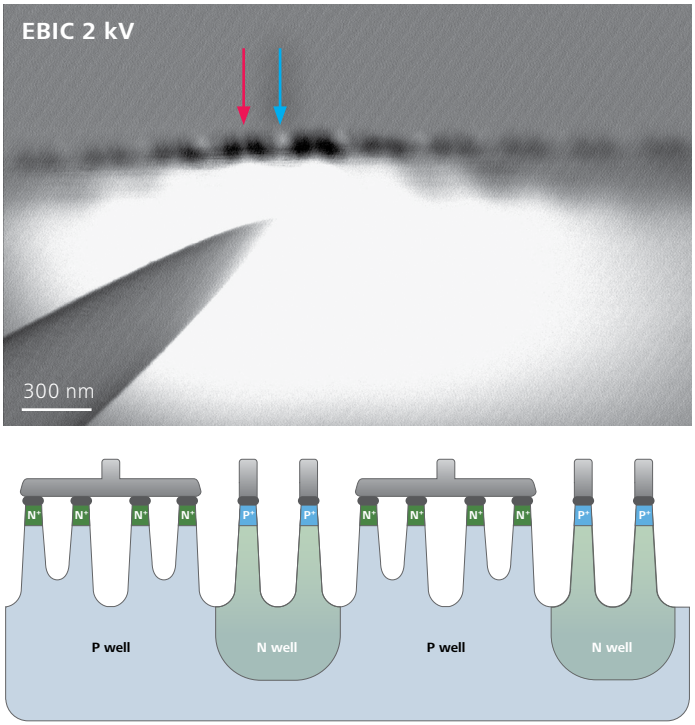

Figure 5 *Top: Higher magnification EBIC image taken on the 30 kV cell. From here, the shape of the fins is just visible. Two different contrasts are seen, (arrows) indicating successful EBIC detection of both n/p and p/n junctions' depletion zones. Bottom: pattern of N^+, P^+, NW, and PW shapes that correspond to the pattern observed above.*

Second Lamella Preparation

The second experiment was designed to look at leakages as a function of Ga-FIB polish. A second lamella was prepared from the 5 nm SRAM sample, this time choosing a plane in a logic area which intersects the gates and also contains several higher-metal regions for probing. Again, a series of cumulative FIB polishes were undertaken, where the final polishes were of the values 30 kV, 5 kV, 2 kV, and 500 V. EBIC measurements were now undertaken at two different beam landing energies on different BEOL parts of the array. One typical plane of view is shown in Figure 6.

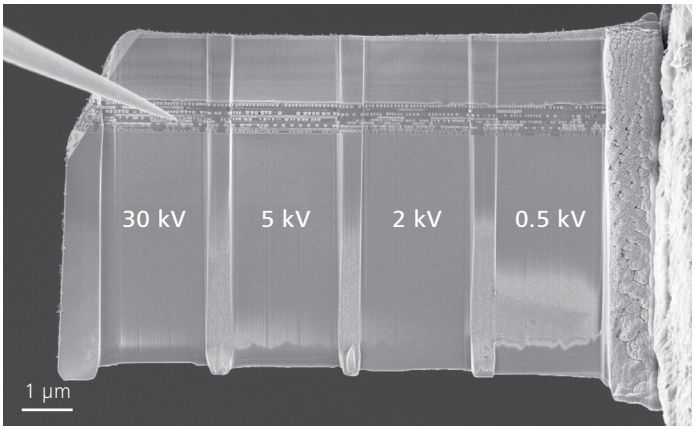

Figure 6 *Second lamella prepared. View of the entire lamella showing the four different regions of Ga-FIB polish.*

Second Lamella Results

At this point, a brief explanation about the EBAC technique would be helpful to justify the motivation for the design of this part of the experiment. EBAC measurements are very sensitive to current leakages in a sample. Consider a typical EBAC setup as depicted in Figure 7, where the beam conditions are chosen such that there is a net loss of electrons from the surface metal features. This loss of electrons is re-supplied by the grounded probing needle and recorded as EBAC/EBIC current. However, if there were any leakages across the surface of the lamella, then the bulk of the sample could also supply electrons to replace those lost by secondary emission. Thus, the magnitude of the EBIC signal would be reduced. This effect would have more noticeable at low beam currents.

With respect to the Ga-FIB preparation, this means that any implantation decreasing the resistance at the sample surface will have an impact on the measured EBIC current. Thus, EBIC current measurements may be used as a proxy for detecting shorts due the sample prep.

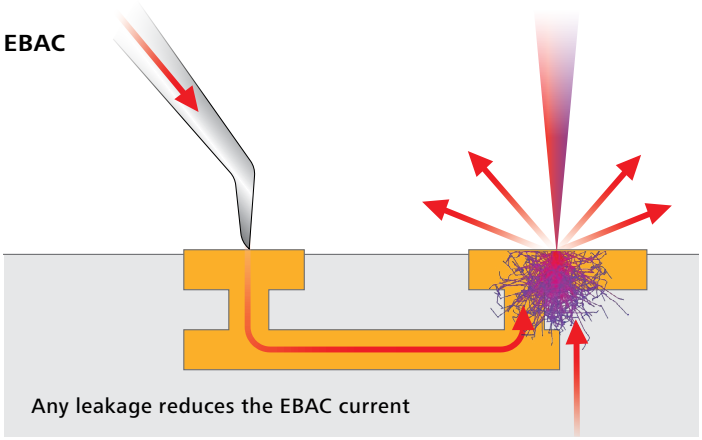

Figure 7 *Diagram indicating how leakage currents in the sample may affect the measured EBAC current.*

Typical EBIC measurements for the procedure on the second lamella are presented in Figure 8. The probe is landing on a Metal 1 contact which is connected to features deeper in the sample, behind the gate. The experimental cell involved a final polish of 5 kV Ga^+ beam, but the analysis is performed with a 1 kV SEM beam. The line profile of EBIC data (bottom, Figure 8) shows that there is a real connection across the full width of the contacted copper feature (black in EBIC). At the same time, the same background current detected across both another metal connector in the structure, and the oxide between them. This result indicates no detectable leakages in the sample.

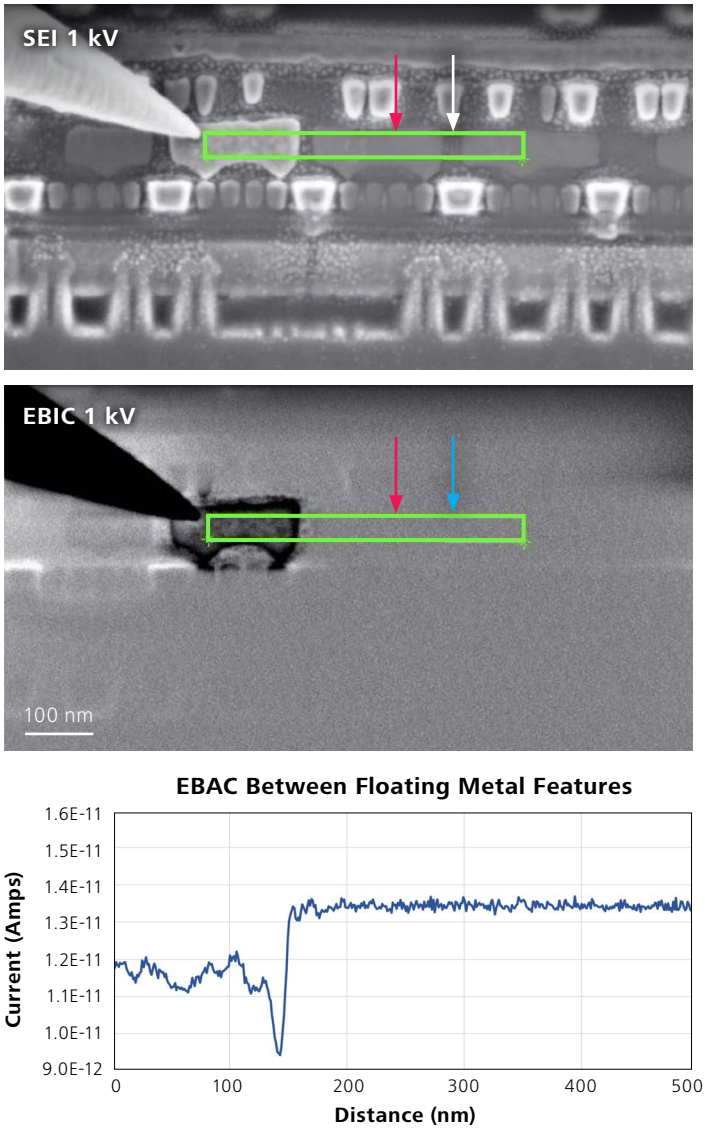

Figure 8 *Areas examined and compared quantitatively on the 5 kV-milled cell. Images show SE image (Top) with marked area and corresponding EBAC image (Middle). The corresponding line trace of current data from the green box is plotted (Bottom).*

Figure 9 shows the full set of experimental cells examined, here including 30 kV, 5 kV, 2 kV, and 0.5 kV. While two high-kV sections only show EBAC effects, the 500 V and 2 kV sections, in contrast, also show EBIC effects from the depletion zones of *p/n* junctions in the two images at the bottom of the Figure. A careful discussion of the details in the 0.5 kV cell would be in order. The corresponding EBIC image at the bottom of the figure reveals two different contrasts. First, a medium-grey, or EBAC, or negative current is detected around the corners of the gate. This indicates connectivity: the beam has wrapped around the gate and its effects are being detected by the system. There is also an EBIC effect, seen as black and white spots, where much larger negative and positive currents are flowing. These signals line up with the fins and are an indication of having reached the depletion zones of the devices behind the gate. This demonstrates the utility of both EBAC and EBIC on a Ga-FIB milled surface.

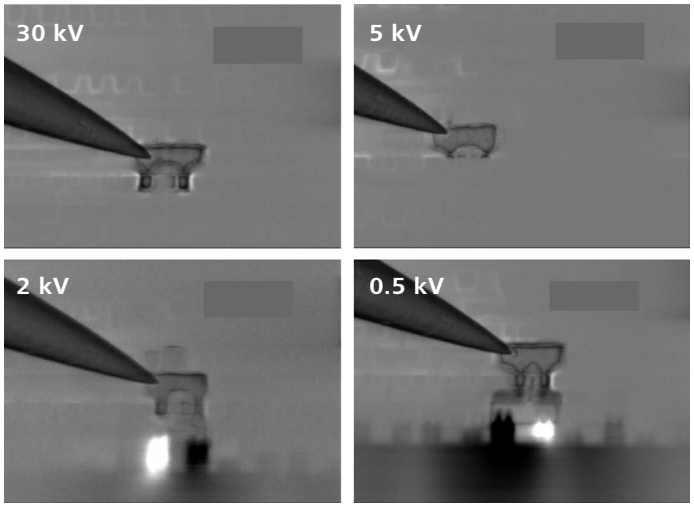

Figure 9 *EBIC/EBAC images from four experimental cells. Different areas of the sample underwent a series of cumulatively increasing number of steps of Ga-FIB polishing, where each step used a decreasing Ga^+ beam energy. The measurements, with needle landing on a Metal 1 contact, were taken with a 1 kV electron beam. Across the four cells, there are different signals. The grey signal of the 30 kV and 5 kV cells may be referred to as "EBAC" as it only gives information about continuity. At 2 kV and 500 V, however, the black and white spots are true EBIC, indicating an imaging of the* p/n *junctions of opposite polarities, these being "behind" the gate in the depth of the sample.*

In order to quantify further any possible influence of a possible Ga^+ implantation or re-deposition, the difference between the EBAC current of the contacted area and a non-contacted area was measured (Figure 8). As the current of a non-contacted area flows to the substrate and not to the current amplifier, we can assume that any leakage caused by the preparation will be detected by the EBAC measurement and an electrical measurement. Both measurements are typical methods used in failure analysis and are therefore taken into account.

The contacted and non-contacted area EBAC currents are each spatially averaged and plotted as line plots — one example is seen in Figure 8 — using the Kleindiek Nanotechnik EBIC Overlay Tool. The results of each section are shown in Table I.

	Energy of Final Ga-FIB polish			
	30 kV	5 kV	2 kV	500 V
Average	9.3 pA	8.7 pA	11.8 pA	8.5 pA
σ contact	2.2 pA	1.1 pA	1.7 pA	1.7 pA
σ bulk	0.6 pA	0.1 pA	0.3 pA	0.2 pA

Table 1 *Overview of the EBAC results. $\sigma_{contact}$ is the standard deviation of the contacted area, σ_{bulk} that of the non-contacted region.*

Finally, a direct electrical measurement of the leakage was done at an insulated contact with no connection to a *p/n* junction or the substrate (Figure 10). The corresponding I-V curve, measured with a Keithley 4200-SCS, is shown in Figure 11, showing extremely little current.

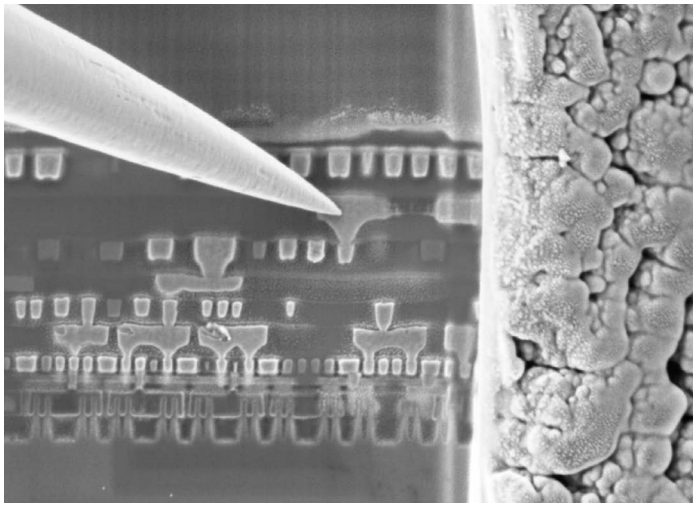

Figure 10 *SE image showing the insulated contact of the leakage measurement.*

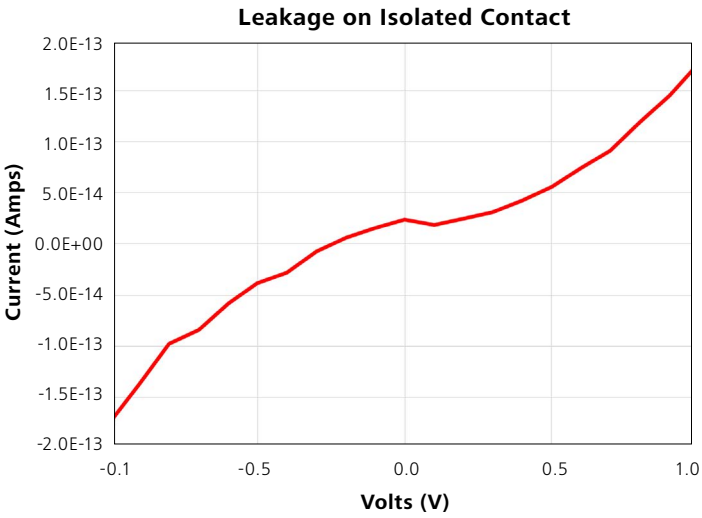

Figure 11 *I-V curve of an isolated contact, showing practically no current at all, indicating no leakage.*

Conclusions

A 5 nm SRAM was cross sectioned by Ga-FIB milling to expose various surfaces. In one experiment, a range of FIB polishes were undertaken, and the surface exposed both the fins and N-wells in cross section. Within one field of view, it was possible to examine multiple FIB treatments at the same time. Meaningful EBIC data, sensitive enough to capture signals from both N-well and P-wells, was detected. This was across a 20 µm field of view with a single probe drop. There was little difference in the ability to image depletion zones in a sample across various surface treatments. It is also likely that the interaction volume of the electron beam in the sample is much larger than any amorphization zone, even in this 30 kV experimental cell.

A second experiment tested concerns about leakage, or shorting, within the plane of the lamella. Measurements were taken by placing the probe needle on contacts in the BEOL wiring. True EBIC data related to imaging of the depletion zones was seen in the sample. These results provide proof of being able to use EBIC analysis on Ga-FIB-milled samples in complicated, even "hard to reach" areas of a sample.

In addition, a quantitative estimation of the influence of the Ga-FIB preparation can be done by considering the EBAC currents. From the EBAC measurement we can clearly distinguish between the contacted elements that appear dark and the rest of the lamella which is grey. The difference in current was measured to be around 10 pA. If Ga^+ implantation or re-deposition were to have shorted the insulated gate with the bulk silicon, the EBAC image would have detected features outside of the contacted gate connections. Indeed, we see some structures outside the gate, however, these can be attributed to the secondary electron emission of the sample reaching the probe needle. The noise level in the region outside the gate is around 100 - 200 fA. Given a lack of EBIC signal outside the gate, there is evidence that the actual leakage current is unlikely to be above 200 fA.

This was verified with the electrical measurement that shows a leakage of 180 fA/V, a value which according to current experience is expected within normal leakages for a 5 nm technology node semiconductor device. Therefore, it is concluded that the influence of the Ga-FIB preparation on electrical leakage measurements and EBAC/EBIC imaging is negligible.

It is always important to distinguish between metrology and defect localization when considering characterization and FA techniques. If the only purpose of a measurement were to derive quantitative measurements of dopant levels in a sample, as one example, then other techniques which do not involve Ga^+ exposure could be used by those with such concerns. However, for the goals of defect localization, then one merely has to identify an anomaly in the field of view.

The results of this paper successfully demonstrate that the use of Ga-FIB milling does not detrimentally impact the ability to perform nanoprobing or EBIC measurements; the results are well within the sensitivities needed for failure analysis and device characterization.

It should be noted that other work with techniques that are more surface sensitive, such as scanning spreading resistance microscopy (SSRM) and scanning capacitance microscopy (SCM), have been shown [9] to suffer a greater effect from Ga^+ milling than has been presented here with EBIC. It was suggested that the effect was due to dopant deactivation during milling and not directly related to the presence of gallium. EBIC, meanwhile, is a volume technique, being a property of the interaction volume of the SEM beam with the sample. Since EBIC appears less hindered by surface conditions, it may provide a truer reading of the electrical state.

Future Work

A similar experiment could be carried out in the SRAM array, in a plane of view where both NFET and PFET devices are visible, where source/drain contacts are exposed. Furthermore, some unpublished results of quantitative measurements of leakage currents between features were also undertaken, which further provided evidence against Ga^+ shorting of the surface features. These data may be developed in a future paper.

References

[1] E. Sperling and S. Rambo, "Reliability Challenges Grow for 5/3 nm," *Semiconductor Engineering,* no. 7 April 2020.

[2] J.-S. Yoon, J. Jeong, S. Lee and R.-H. Baek, "Sensitivity of Source/Drain Critical Dimension Variations for Sub-5-nm Node Fin and Nanosheet FETs," *IEEE Transactions on Electron Devices,* vol. 67, no. no. 1, pp. 258-262, 2020.

[3] E. Hendarto and et al., "Investigation of soft fail issue in sub-nanometer devices using nanoprobing technique," *15th International Symposium on the Physical and Failure Analysis of Integrated Circuits, Singapore,* no. doi: 10.1109/IPFA.2008.45, 2008.

[4] H. Faraby, T. Deborde and M. von Haartman, "Efficient Fault Isolation and Failure Analysis Methods to Root Cause Defects in Microprocessors.," *Proceedings of the ISTFA 2019,* no. https://doi.org/10.31399/asm.cp.istfa2019p0377, pp. 377-380.

[5] Z. Song, P. McGinnis, D. Albert, G. Hornicek, M. Tenney, L. Fischer, J. Sylvestri, P. Tran, C. Le, D. Floyd, G. Lian, S. Boettcher and M. Ali, "Electrical Probing Role in 14nm SOI Microprocessor Failure Analysis.," *Proceedings of the ISTFA 2020,* no. https://doi.org/10.31399/asm.cp.istfa2020p0061, pp. 61-66.

[6] "Transmission electron microscopy," Wikipedia, [Online]. Available: https://en.wikipedia.org/wiki/Transmission_electron_microscopy.

[7] W. A. Hubbard, L. J. J., H. L. Chan, M. M. Mecklenburg and B. C. Regan, "Nanoscale Conductivity Mapping: Live Imaging of Dielectric Breakdown with STEM EBIC," *IEEE International Symposium on the Physical and Failure Analysis of Integrated Circuits (IPFA),* no. doi: 10.1109/IPFA55383.2022.9915733, pp. 1-4, 2022.

[8] K. Pandey, K. Paredis, T. Hantschel, C. Drijbooms and W. Vandervorst, "The impact of focused ion beam induced damage on scanning spreading resistance microscopy measurements," *Sci Rep,* vol. 10, p. 14893, 2020.

[9] K. Pandey, K. Paredis, T. Hantschel and e. al., "The impact of focused ion beam induced damage on scanning spreading resistance microscopy measurements," *Sci Rep,* vol. 10, no. 2020, p. 14893.

[10] M. Presley, "The Formation of Amorphous and Crystalline Damage in Metallic and Semiconducting Materials under Gallium Ion Irradiation," The Ohio State University, Columbus, OH, 2016.

[11] A. Qiu, W. Lowe and M. Arora, "NanoProbing on 7 nm FinFET Devices in an SRAM Array: Challenges and Solutions," *ISTFA,* no. DOI: 10.31399/asm.cp.istfa2019p0329, 2019.

[12] G. Johnson and R. A., "Unpacking the nanoprobing signals that arise from electron beam interactions with electronic devices," in *EDFAS Lone Star Chapter Meeting,* 2022.

[13] J. R. Beall and L. C. Hamiter, "EBIC - A Valuable Tool for Semiconductor Evaluation and Failure Analysis.," *15th International Reliability Physics Symposium,* pp. 61-69, 1977.

[14] G. Johnson, A. Rummel and H. Stegmann, "In-situ EBIC measurements of IGBT during device turn-on," *IPFA,* 2023.

[15] G. M. Johnson, H. Stegmann, T. Rodgers, F. Hitzel, A. Rummel, D. Mello and M. Kuball, "In-Situ Junction Analysis in SiC (and GaN)," *Conference Proceedings from the 49th International Symposium for Testing and Failure Analysis,* no. https://doi.org/10.31399/asm.cp.istfa2023p0509, pp. 509-518, 2023.

[16] G. Johnson, J. Nxumalo, A. Arya, J. Johnson, Q. Gao and B. Greene, "Innovative use of FA techniques SCM and OBIRCH along with TCAD to resolve junction scaling issues at advanced technology nodes," *29th Annual SEMI Advanced Semiconductor Manufacturing Conference (ASMC),* no. doi: 10.1109/ASMC.2018.8373206., pp. 370-373, 2018.

[17] G. Johnson, H. Stegmann and A. Rummel, "Zero Channel Bias Determination of Device Turn-On and the Seebeck Effect in Nanoprobing," *Conference Proceedings from the 48th International Symposium for Testing and Failure Analysis,* no. https://doi.org/10.31399/asm.cp.istfa2022p0262, pp. 262-268, 2022.

Carl Zeiss Microscopy GmbH
07745 Jena, Germany
microscopy@zeiss.com
www.zeiss.com/semiconductor-microscopy

Follow us on social media: